2001

Biotransformation of Ni-Substituted Hydrous Ferric Oxide by an Fe(III)-Reducing Bacterium

James K. Fredrickson
Pacific Northwest National Laboratory, jim.fredrickson@pnl.gov

John M. Zachara
Pacific Northwest National Laboratory

Ravi K. Kukkadapu
Pacific Northwest National Laboratory, ravi.kukkadapu@pnl.gov

Yuri A. Gorby
Pacific Northwest National Laboratory

Steven C. Smith
Pacific Northwest National Laboratory

See next page for additional authors

Environ. Sci. Technol. **2001**, *35,* 703−712

Biotransformation of Ni-Substituted Hydrous Ferric Oxide by an Fe(III)-Reducing Bacterium

JAMES K. FREDRICKSON,*
JOHN M. ZACHARA,
RAVI K. KUKKADAPU, YURI A. GORBY,
STEVEN C. SMITH, AND
CHRISTOPHER F. BROWN

Pacific Northwest National Laboratory, P.O. Box 999, MSIN P7-50, Richland, Washington 99352

The reductive biotransformation of a Ni^{2+}-substituted (5 mol %) hydrous ferric oxide (NiHFO) by *Shewanella putrefaciens*, strain CN32, was investigated under anoxic conditions at circumneutral pH. Our objectives were to define the influence of Ni^{2+} substitution on the bioreducibility of the HFO and the biomineralization products formed and to identify biogeochemical factors controlling the phase distribution of Ni^{2+} during bioreduction. Incubations with CN32 and NiHFO were sampled after 14 and 32 d, and both aqueous chemistry and solid phases were characterized. By comparison of these results with a previous study (Fredrickson, J. K.; Zachara, J. M.; Kennedy, D. W.; Dong, H.; Onstott, T. C.; Hinman, N. W.; Li, S. W. *Geochim. Cosmochim. Acta* **1998**, *62*, 3239−3257), it was concluded that coprecipitated/sorbed Ni^{2+} inhibited the bioreduction of HFO through an undefined chemical mechanism. Mössbauer spectroscopy allowed analysis of the residual HFO phase and the identity and approximate mass percent of biogenic mineral phases. The presence of AQDS, a soluble electron shuttle that obviates need for cell−oxide contact, was found to counteract the inhibiting effect of Ni^{2+}. Nickel was generally mobilized during bioreduction in a trend that correlated with final pH, except in cases where PO_4^{3-} was present and vivianite precipitation occurred. CN32 promoted the formation of Ni^{2+}-substituted magnetite ($Fe^{III}_2Fe^{II}_{(1-x)}Ni^{II}_xO_4$) in media with AQDS but without PO_4^{3-}. The formation of this biogenic coprecipitate, however, had little discernible impact on final aqueous Ni^{2+} concentrations. These results demonstrate that coprecipitated Ni can inhibit dissimilatory microbial reduction of amorphous iron oxide, but the presence of humic acids may facilitate the immobilization of Ni within the crystal structure of biogenic magnetite.

Introduction

As reactive components of soils and sediments, iron oxides can have an important role in controlling the behavior of trace metal cations such as Ni and Co. For example, metal cations can be strongly sorbed to iron oxide surfaces with the strength and extent of sorption being a function of factors that include metal cation type, pH, oxide mineralogy, and surface area. Also di-, tri-, and tetravalent metals may substitute for Fe to varying degrees in the structures of iron oxides; hence, the fate of the substituting metal cation is intimately tied to reactions controlling the formation and dissolution of the oxide. For example, in recent investigations, we examined the fate of Co and Fe in suspensions of a Co-substituted goethite ($Co_{0.01}Fe_{0.99}OOH$) subjected to bioreduction by *Shewanella putrefaciens* CN32 (*2*). Co(III) was reduced by the bacterium to Co(II) at concentrations, relative to Fe(II), proportional to its mole ratio in the oxide. The extent of solubilization of the bioreduced Co(II) was dependent upon multiple factors that included buffer type, the presence or absence of P, and the extent of reduction of the Co−FeOOH. Co(II) behavior was linked to competitive sorption reactions on the Co−FeOOH surface and coprecipitation in biogenic Fe(II) minerals. In similar studies investigating the bacterial reduction of metal-substituted goethites, the rates of bacterial dissolution of Mn-, Co-, Al- or Cr-substituted goethites were slower relative to an unsubstituted goethite (*3*), and only Mn and Co were solubilized at concentrations that were congruent with respect to Fe.

Amorphous hydrous iron oxide (HFO) is common in soils and sediments that undergo periodic cycling between oxidizing and reducing conditions and therefore are not subject to processes such as aging, dehydration, or heating that promote transformation to more crystalline phases. Although iron-reducing bacteria (DIRB) such as *S. putrefaciens* can utilize both crystalline and poorly crystalline iron oxides as electron acceptors (*4*−*7*), poorly crystalline iron oxides are more bioavailable relative to crystalline phases and are believed to be the principal forms of Fe(III) reduced by bacteria in anoxic sediments (*8*). Due to their amorphous structure and relatively high surface areas, poorly crystalline oxides have a high capacity for sequestering metal cations (*9*−*11*). However, as amorphous iron oxides convert to more crystalline forms either during aging or exposure to alkaline conditions, the transformation products may have an increased or reduced capacity for trace metal sequestration. Despite the potential importance of these processes, relatively little is known about the fate of associated trace metals during the microbial reduction of HFO (*12*).

The purpose of this research was to investigate the bioreduction of Ni-substituted HFO ($Ni_{0.05}Fe_{0.95}$) by *S. putrefaciens* during anaerobic respiration and the partitioning of the associated Ni^{2+} and Fe(II) into aqueous and solid phases as a function of buffer type and solution composition. The influence of Ni^{2+} on the bioreduction process is explored along with effects of PO_4^{3-} on biomineralization. Insights are provided into the phases controlling the solubility and, therefore, relative mobility of oxide-associated Ni^{2+} as the coprecipitate is biologically reduced. This information contributes to the current understanding of the role of bacterially mediated transformations on the cycling of trace metals and the fate of metal contaminants in soils and sediments.

Materials and Methods

NiHFO was prepared similar to the procedure described by ref *13* using nitrate salts. Following precipitation at pH 7, the NiHFO suspension was "aged" at room temperature under an anoxic atmosphere for approximately 13 months. The Ni^{2+} content of the final product was 5 mol % or 0.05 mol of Ni^{2+}/mol of Fe. This value was well below the overall sorption capacity of HFO (0.2 mol/mol Fe) (*14*). The nitrate concentration in the solution was reduced to <1 mg L^{-1} nitrate by extensive washing with anoxic 0.1 mol/L $NaClO_4$.

* Corresponding author phone: (509)376-7063; fax: (509)376-1321; e-mail: jim.fredrickson@pnl.gov.

10.1021/es001500v CCC: $20.00
Published on Web 01/11/2001

Triplicate anoxic NiHFO (50 mmol of Fe(III)/L) suspensions were pH adjusted to range from pH 6.0 to pH 9.0 in 0.5-unit increments using dilute anoxic HCl or NaOH. Two electrolyte solutions were utilized: (i) 28 mmol/L NH_4Cl, 30 mmol/L lactate, and 50 mmol/L $NaClO_4$ or (ii) the same as i but including 4.3 mmol/L P (as NaH_2PO_4). The pH was adjusted on day 1 and readjusted on day 2, the aqueous phase was sampled for Ni^{2+}(aq) and PO_4^{3-}, and the final pH was determined on day 3. The suspensions were mixed at 30 °C and 100 rpm. Phase separation was accomplished by transferring 3 mL of suspension to a syringe fitted with a 0.2-μm syringe filter unit. The first 1 mL of filtrate was discarded, and the remaining filtrate was collected for analysis of Ni^{2+}(aq) and PO_4^{3-} by ICP-MS. The experiment was conducted and sampled under an anoxic atmosphere to mimic the conditions of other experiments.

Anoxic suspensions of *S. putrefaciens* strain CN32 were prepared and used in a manner identical to previous research (*7*). Media components included (in mmol/L): NH_4Cl, 28; KCl, 1.34; $CaCl_2$, 0.68; $NaClO_4$, 50; lactate, 30; NaH_2PO_4, 0 or 4.3; and AQDS, 0 or 0.1. Buffers were either 30 mM $NaHCO_3$ or PIPES, and headspace atmospheres were either 100% N_2 (PIPES) or 80:20% N_2:CO_2 ($NaHCO_3$). The media were filter sterilized using a 0.2-μm syringe filtration system after pH adjustment to 6.8 with NaOH.

Samples of the aqueous phase were obtained under an anoxic atmosphere by directly combining 1 mL of 0.2-μm suspension filtrate with 1 mL of anoxic 1 mol/L HCl. Sorbed Fe(II) and Ni^{2+} and weak acid-soluble Fe(II)/(III) and Ni^{2+} were obtained by combining 0.2 mL of suspension with 3.8 mL of anoxic 0.53 mol/L HCl, termed the 0.5 mol/L HCl extraction, and incubating at 30 °C with agitation for approximately 24 h. Phase separation of the weak acid extract was accomplished using a 0.2-μm syringe filter. The first 1 mL of filtrate was discarded. Total Fe(II+III) and Ni^{2+} were obtained by combining 1 mL of suspension with 0.7 mL of concentrated Ultrex HCl, termed the 5 mol/L HCl extraction. Complete dissolution of the solid phase in 5 mol/L HCl was achieved within 24 h. The suspension pH was determined under an anoxic atmosphere using a glass combination pH microelectrode (Microelectrodes, Inc., Bedford, NH).

To probe whether Ni^{2+} could potentially inhibit Fe(III) reduction by *S. putrefaciens* CN32, two experiments were conducted, one with Fe(III)−nitrilotriacetic acid (NTA), a soluble form of Fe(III) that is readily reduced by CN32, and unsubstituted HFO, also readily reduced by CN32. For the experiments evaluating the effect of Ni on Fe(III)−NTA reduction, cultures consisted of CN32 at a cell concentration of 3×10^8 cells mL^{-1}, 10 mmol/L Fe(III)−NTA, 30 mmol/L each sodium lactate, and pH 7 bicarbonate buffer. Treatments consisted of untreated cells and Fe(III)−NTA with or without the concurrent addition of 0.5 mmol/L Ni, as $NiCl_2 \cdot 6H_2O$, and CN32 cells preincubated in 0.5 mmol/L Ni^{2+} solution for 2 h and washed 1× in pH 7 bicarbonate buffer and either Fe(III)−NTA or Fe(III)−NTA with 0.5 mmol/L Ni^{2+}. A similar experiment was conducted with 50 mmol/L HFO substituting for the Fe(III)−NTA.

The concentrations of Fe(II) and Fe(total) were determined on all bioreduced and control samples using the ferrozine assay (*15*, *16*). The determination of Fe(II) in samples was accomplished within 2 h of sampling. The concentrations of Ni and Fe were also determined using ICP-MS.

Mössbauer Spectroscopy. Random orientation absorbers were prepared by mixing 17−28 mg of dried sample, prepared by filtering solids from suspensions and washing with acetone, with petroleum jelly in a 0.5 or 3/8 in. thick and 0.5 in. i.d. Cu holder sealed at one end with clear scotch tape. The sample space was filled with petroleum jelly, and the ends were sealed with the tape. The bioreduced samples were handled under an anaerobic atmosphere. Spectra were collected at room temperature (RT) using ~50 mCi (1.85 MBq) (initial strength) ^{57}Co/Rh single-line thin sources. The Mössbauer bench (MB-500; WissEL, Germany) was equipped with a dual Mössbauer drive system to gather data simultaneously for two experiments. The velocity transducer (MVT-1000; WissEL) was operated in the constant-acceleration mode (23 Hz, ±10 mm/s). Data were acquired on 1024 channels and then folded to 512 channels to give a flat background and a zero-velocity position corresponding to the center shift (CS or δ) of a metallic iron foil at room temperature. Calibration spectra were obtained with a 20-μm-thick α-iron foil (Amersham, England) placed in exactly the same position as the samples to minimize any error due to changes in geometry. The transmitted radiations were recorded with Ar−Kr proportional counters. The unfolded spectra obtained were folded and evaluated with the Recoil program (University of Ottawa, Canada) using a Voigt-based hyperfine parameter distribution method (*17*).

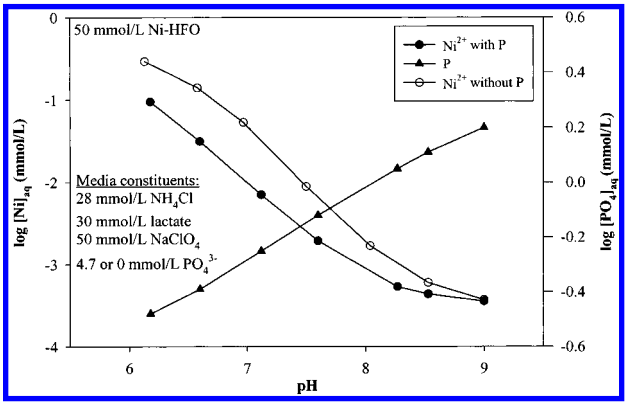

FIGURE 1. Solubility of Ni^{2+} in contact with NiHFO (50 mmol/L) and major media components as a function of pH in the presence and absence of added PO_4^{3-} (4.7 mmol/L).

The Mössbauer spectrum measured at room temperature (see Figure 1a in Supporting Information) showed a symmetric doublet (δ = 0.36 mm/s and ΔE_q = 0.69 mm/s) indicative of a poorly crystalline material. The Mössbauer spectrum is sensitive to the presence of goethite and hematite, and the presence of these crystalline phases was not observed. X-ray diffraction analyses also revealed lower crystallinity of the NiHFO, with evidence of only 2−3 broad lines in its spectrum (see Figure 1b in Supporting Information). The peaks at 35.5° and 62.5° were from HFO. More crystalline ferrihydrites have six lines in their XRD patterns.

Results

Chemical Behavior of the NiHFO. Previous studies have shown that coprecipitated metals with and adsorbed metals on HFO behave comparably in terms of adsorption/desorption behavior (*14*). Phosphate (4.7 mmol/L) added to the incubation media sorbed to the NiHFO (Figure 1). Its sorption behavior was characteristic of an anion, increasing with decreasing pH and increasing positive surface charge on the sorbent (*14*). At pH 7.15, the initial PO_4^{3-} concentration of 4.7 mmol/L was decreased to 0.58 mmol/L by adsorption. The coprecipitated Ni^{2+} showed contrasting behavior to PO_4^{3-} but typical of that of a cationic metal (*14*), with sorption increasing with increasing pH (Figure 1). A one-unit variation in pH in the circumneutral pH region leads to a log unit change in Ni^{2+}(aq). The presence of media PO_4^{3-} decreased Ni^{2+}(aq) concentrations maintained by the HFO (Figure 1) by approximately 0.5 log unit, indicating an increase in Ni^{2+} sorption/retention by the solid phase. This enhanced Ni^{2+} sorption may result from an increase in negative surface charge density resulting from sorbed PO_4^{3-}; ternary surface complex formation between FeOH surface sites, PO_4^{3-} and

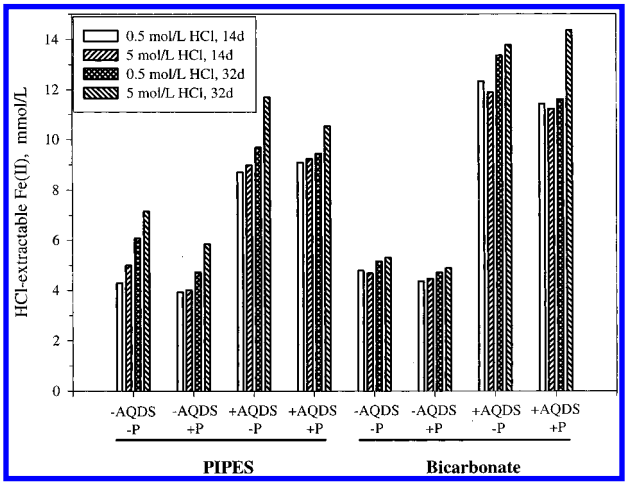

FIGURE 2. Concentration of Fe(II) in 0.5 and 5.0 mol/L HCl extracts of bioreduced NiHFO after 14 and after 32 d incubation at 30 °C.

Ni^{2+}; or surface coprecipitation. Fe(II) sorbs comparably, but more strongly, to HFO than does Ni^{2+} (*7*).

NiHFO Reduction by *S. putrefaciens*. The extent of bioreduction of NiHFO was determined by measuring Fe(II) extracted by dilute (0.5 mol/L) and strong (5.0 mol/L) HCl. These two extraction methods were employed because a variety of phases can be generated as a result of bioreduction of HFO, including acid-soluble phases such as siderite ($FeCO_3$) and vivianite [$Fe_3(PO_4)_2 \cdot 8H_2O$] and crystalline iron-(III) oxides including magnetite (Fe_3O_4) and goethite (α-FeOOH) that are poorly soluble in 0.5 mol/L HCl (*18*).

Solution composition, buffer type, and the presence of anthraquinone-2,6-disulfonate (AQDS) in particular strongly influenced the extent of NiHFO reduction. The presence of 0.1 mmol/L AQDS had the most striking effect on NiHFO reduction resulting in a 1.6−3-fold increase in HCl-extractable Fe(II), regardless of buffer type (Figure 2). The influence of PO_4^{3-} on bioreduction was less extensive but resulted in less HCl-extractable Fe(II) in those treatments with AQDS. There was little difference in the amount of Fe(II) in the 0.5 and 5.0 mol/L HCl extracts at 14 d, but at 32 d the 5.0 mol/L HCl consistently extracted more Fe(II) than did the more dilute acid (Figure 2). This was particularly pronounced in the PIPES-buffered treatments where 10−19% more Fe(II) was extracted by the strong acid (Figure 2). In previous studies (*7*), unsubstituted and unaged HFO was reduced by CN32, in general, to a greater degree than the NiHFO. In the bicarbonate-buffered no-cell controls in this study, HCl-extractable Fe(II) was near the detection limit of the ferrozine assay for the dilutions measured and ranged from 0.09 to 0.23 mmol of Fe(II)/L.

The amount of Ni^{2+} in the HCl extracts of the bioreduced NiHFO after 32 d incubation closely tracked total Fe (II+III) (see Figure 2 in Supporting Information). The proportion of metal, Fe or Ni, extracted by 0.5 mol/L HCl was consistently less than that extracted by 5.0 mol/L HCl, but the differences were greatest in those treatments that lacked PO_4^{3-}. These results indicated that there was a greater proportion of crystalline mineral phases forming upon incubation, particularly in the absence of PO_4^{3-}, and that the Ni^{2+}, to the same extent as for Fe(II), was being incorporated into the crystalline phases. Consistent with the XRD and Mössbauer spectrum (see Figure 1 in Supporting Information), approximately 99% of the total Fe and 94% of the total Ni associated with the uninoculated (control) NiHFO were soluble in 0.5 mol/L HCl indicating that the aged material had not undergone significant conversion to more crystalline phases.

Bioreduction-Induced Solubilization of Metals. Concentrations of soluble Ni^{2+} and Fe(II) were determined, at 14 and 32 d post-inoculation, on solutions passing a 0.2-μm filter. Previous results from experiments investigating the bacterial reduction of freshly precipitated HFO demonstrated that there was no difference in the Fe(II) concentrations of 0.2-μm or 1.8-nm filtrates (*7*). As observed for the HCl-extractable metals, Ni^{2+}(aq) closely tracked Fe(II)(aq) but at concentrations ranging from 7 to 23% of those for Fe(II)(aq) (Figure 3). At both sampling times, the concentrations of soluble metals were higher in the bicarbonate than in the PIPES-buffered solutions, and the presence of PO_4^{3-} consistently resulted in lower Ni^{2+}(aq) and Fe(II)(aq). The presence of AQDS did not have a consistent significant effect on the concentration of Fe(II)(aq) or Ni^{2+}(aq) as it did on HCl-extractable Fe(II) (Figure 2). Fe(II) and total Fe in unreduced controls were below detection limits (<3 μmol/L) while Ni^{2+} ranged from 74 to 109 μmol/L.

The aqueous concentrations of Fe(II) and Ni^{2+} were not well correlated with the total extent of reduction as defined by HCl extraction (Figure 2). While the treatment exhibiting one of the largest extents of reduction (bicarbonate, +AQDS and PO_4^{3-}) showed the largest concentrations of Fe(II)(aq) and Ni^{2+}(aq) (Figure 3), other treatments showing extensive reduction did not. The treatment showing the second greatest concentrations of F(II)(aq) and Ni^{2+}(aq) (Figure 3; bicarbonate, −AQDS and PO_4^{3-}) exhibited the lowest extent of

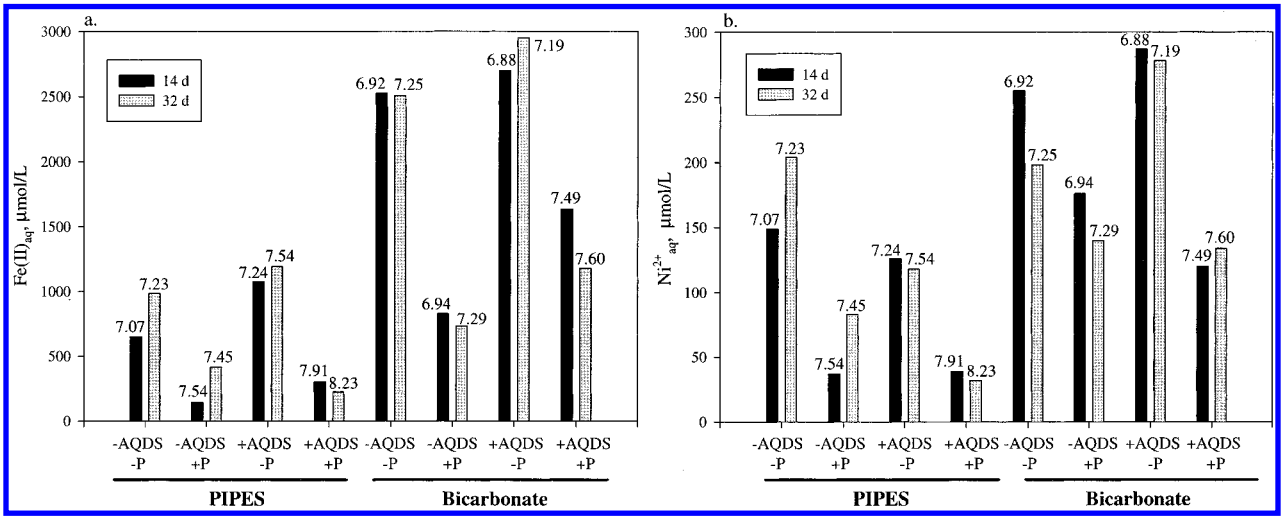

FIGURE 3. Concentrations of aqueous (0.2 μm filtered) Fe(II) and Ni^{2+} in bioreduced NiHFO suspensions following incubation for 14 and 32 d. Note average final pH values recorded above each treatment.

bioreduction (Figure 2). A reasonable correlation, however, was noted between Fe(II)(aq) and Ni^{2+}(aq) and pH (note final pH values in Figure 3b). Consistent with Figure 1, incubations with lower final pH tended to have higher concentrations of both Fe(II)(aq) and Ni^{2+}(aq) than did those with high final pH.

Biomineralization of NiHFO. The XRD analyses of the bioreduced solids revealed extensive biomineralization in some treatments and little or none in others. Those solutions that lacked PO_4^{3-} but contained AQDS, in either buffer, underwent the greatest biomineralization (Figure 4, panels b and f). The biotransformed NiHFOs contained crystalline solids dominated by magnetite (Fe_3O_4) or a magnetite-like phase as inferred from the XRD patterns (*d* spacings). Bioreduced NiHFO in HCO_3^- buffer without AQDS or PO_4^{3-} showed, apart from broad lines (2−3-line ferrihydrite), peaks due to 6-line ferrihydrite and goethite [20° 2-θ; d_{110}] indicating microbiologic enhancement of the crystallization of HFO (Figure 4a). An XRD pattern collected on solids from this same treatment after only 14 d of incubation contained more goethite than the 32 d material in (Figure 4a). XRD peaks due to other Fe minerals were not evident except for the HCO_3^--buffered solution containing AQDS and PO_4^{3-} (Figure 4d) where several small but well-defined peaks of siderite ($FeCO_3$) and vivianite [$Fe_3(PO_4)_2 \cdot 8H_2O$] were observed. In the PIPES-buffered solution without AQDS or PO_4^{3-}, there was extensive biomineralization of NiHFO to magnetite or a magnetite-like phase (Figure 4e).

^{57}Fe Mössbauer spectroscopy is a relatively sensitive method for characterizing products, even minor phases, resulting from the bacterial reduction of synthetic and natural iron oxides (*19*). In contrast to XRD, it provides information on compounds that do not exhibit long-range structural order (poorly crystalline materials) (*20*). Common Fe minerals such as siderite and vivianite are readily distinguished from each other and from magnetite, goethite, etc. (*21*). Experimental and simulated (Figure 5, panels d and h only) RT Mössbauer spectra of the bacterially reduced NiHFO from the various samples are shown in Figure 5. An intense doublet dominated the spectra of those treatments that also exhibited modest Fe(III) reduction (Figure 5, panels a, c, e, and g) as indicated by HCl-extractable Fe(II) (Figure 2). Their Mössbauer spectra were similar to the doublet for the unreduced NiHFO (see Figure 1 in Supporting Information) although the high energy peak of the ferrous doublet was also evident (noted by *), indicative of <5% bioreduction. The spectra for bioreduced NiHFO samples incubated in bicarbonate or PIPES buffer with AQDS but without PO_4^{3-} (Figure 5, panels b and f) were characteristic of extensive conversion to magnetite, as indicated by poorly resolved sextets typical of tetrahedral and octahedral Fe in a magnetite-like solid. These spectra also displayed a doublet resulting from unreduced NiHFO (~30% spectral area in the sample from the PIPES only treatment). Samples incubated with AQDS and PO_4^{3-} (Figure 5, panels d and h) revealed the presence of vivianite; siderite was also present in the bioreduced NiHFO incubated in bicarbonate buffer with AQDS and PO_4^{3-} (Figure 5d). Simulations indicated that 30% of the spectral area in the HCO_3^--buffered sample with AQDS and PO_4^{3-} was due to a combination of vivianite and siderite while 10% of the area in the PIPES buffer with AQDS and PO_4^{3-} was due to vivianite. Residual NiHFO remained in these treatments at mass concentrations of 70 and 90%, respectively. The two peaks accounting for the vivianite spectra result from two, structurally distinct, Fe(II) site types in vivianite (*22*).

Transmission electron microscopy of the bioreduced NiHFO in PIPES with 100 μM AQDS revealed the presence of randomly distributed nanometer-sized (10−50 nm) crystallites within a matrix of amorphous material (see Figure 3a in Supporting Information). Energy dispersive spectroscopy revealed that the crystallites were comprised mainly of Fe with minor amounts of Ni. HRTEM of the crystallites (see Figure 3b in Supporting Information) provided lattice fringe images with *d* spacings consistent with those for magnetite or a magnetite-like phase.

Effects of Exogenous Ni on Bacterial Reduction of Fe(III)−NTA and HFO. The extent of NiHFO reduction and biomineralization by *S. putrefaciens* CN32 in these experiments was lower by 1.6−5.6-fold for all treatments, except PIPES and PIPES with AQDS, than previous studies with HFO that did not contain Ni^{2+} (*7*). The extensive difference in the reduction between HFO with and without Ni^{2+} prompted investigations into whether the effect was a physiologic or chemical one. In these experiments, the effect of Ni^{2+} on Fe(III) reduction was assessed by adding 0.5 mmol/L $NiCl_2$ to suspensions of CN32 cells that had or had not been preincubated with Ni^{2+} and incubating with either Fe(III)−NTA or HFO in HCO_3^- buffer. The Ni^{2+}(aq) concentrations were undersaturated with respect to $Ni(OH)_2$(c) at the experimental pH values (using solubility data presented by ref *23*).

The presence of 0.5 mmol/L Ni^{2+} had little or no inhibitory effect on the initial rate of reduction of Fe(III)−NTA by CN32; the rate was 17.5 (±0.9) μmol of Fe min^{-1} in the absence of Ni^{2+} and 16.4 (±1.1) μmol of Fe min^{-1} for cultures with Ni^{2+} (Figure 6). In comparison, preincubation of cells with Ni^{2+} resulted in lower initial Fe(III) reduction rates; 13.2 (±0.5) and 11.2 (±0.4) μmol of Fe min^{-1} for cultures without and with 0.5 mmol/L Ni^{2+}, respectively. After 65−70% of the Fe(III) was reduced in the cultures with Ni^{2+} preincubation, the rates of Fe(III) reduction decreased significantly (Figure 6) to between 1.2 (±0.2) and 1.6 (±0.3) μmol of Fe min^{-1}.

In the experiment with HFO, preincubation of cells with Ni^{2+} had no impact on HFO reduction relative to cells not pretreated with Ni^{2+}, while 0.5 mmol/L Ni^{2+} added to HFO suspensions immediately before inoculation with CN32 cells decreased the extent of reduction of HFO by approximately 50% at 15 d (Figure 7). Although the results of the Fe(III)−NTA experiment indicated a modest inhibition of Fe(III) reduction by Ni^{2+} sorbed to cells, the collective results from the Fe(III)−NTA and HFO experiments indicated that the effects were primarily physicochemical in nature as opposed to a general toxic effect on cells or enzyme inhibition.

Discussion

Bioreduction of Aged NiHFO. The extent of HFO reduction and the partitioning of biogenic Fe(II) to solution and solid phases in batch CN32 cultures with HFO is a complex process that is sensitive to numerous factors including pH, rate of bacterial metabolism, electron donor type, and especially solution ion composition (*7*). The partitioning of Fe(II) to the aqueous phase and the nature of biominerals have been, in general, consistent with the phases predicted at equilibrium by thermodynamic calculations. Common biominerals formed from the bacterial reduction of HFO include magnetite, siderite, vivianite, and green rust [iron(II)/iron(III) hydroxide].

The presence of Ni^{2+} coprecipitated with HFO at ~5 mol % and solution composition strongly influenced the extent of NiHFO reduction and its biomineralization by CN32. In comparison to previous experiments with HFO conducted under essentially identical conditions (*7*), the extent of reduction of NiHFO was significantly less, particularly in the bicarbonate buffered solutions and in PIPES with AQDS and PO_4^{3-} (Table 1). Divalent metal cations, such as Ni^{2+} or Co(II), can slow the kinetics of transformation of HFO to crystalline iron oxides and/or change the composition and properties of the end product (*1*). Ni^{2+} and Co(II/III) suppress the transformation of HFO into goethite and/or hematite, by stabilizing the coprecipitate against dissolution (*24*, *25*).

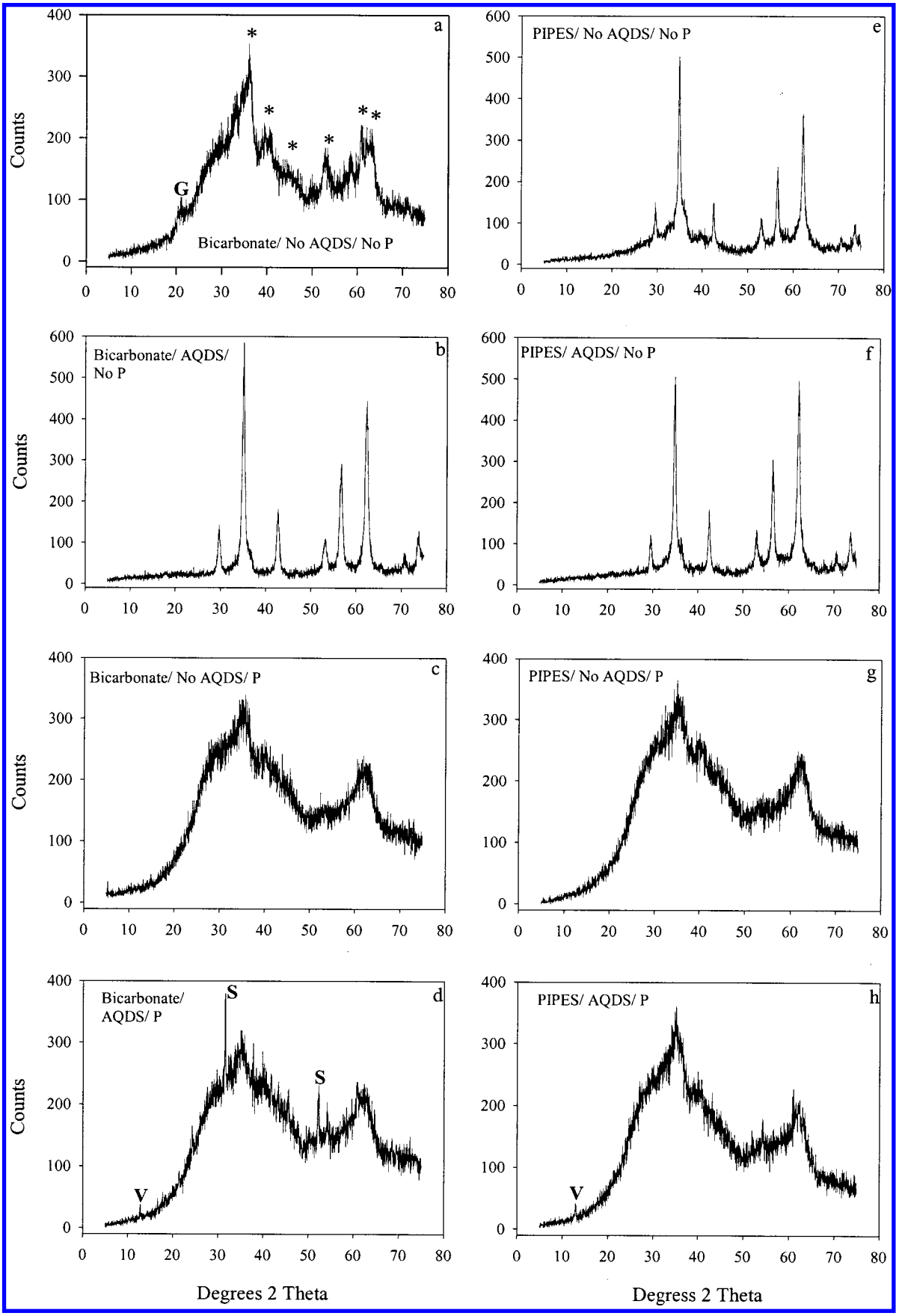

FIGURE 4. Powder X-ray diffraction patterns of bioreduced NiHFO (32 d) in PIPES or bicarbonate-buffered media (*G* = goethite-d_{110}, * = 6-line ferrihydrite peaks, S = siderite peaks, and V = vivianite peaks).

Ni^{2+} was more effective at retarding HFO crystallization than Co(II/III) [or Mn(II/III)] and impacted the rate of crystallization in direct proportion to its concentration in the NiHFO coprecipitate (*24*).

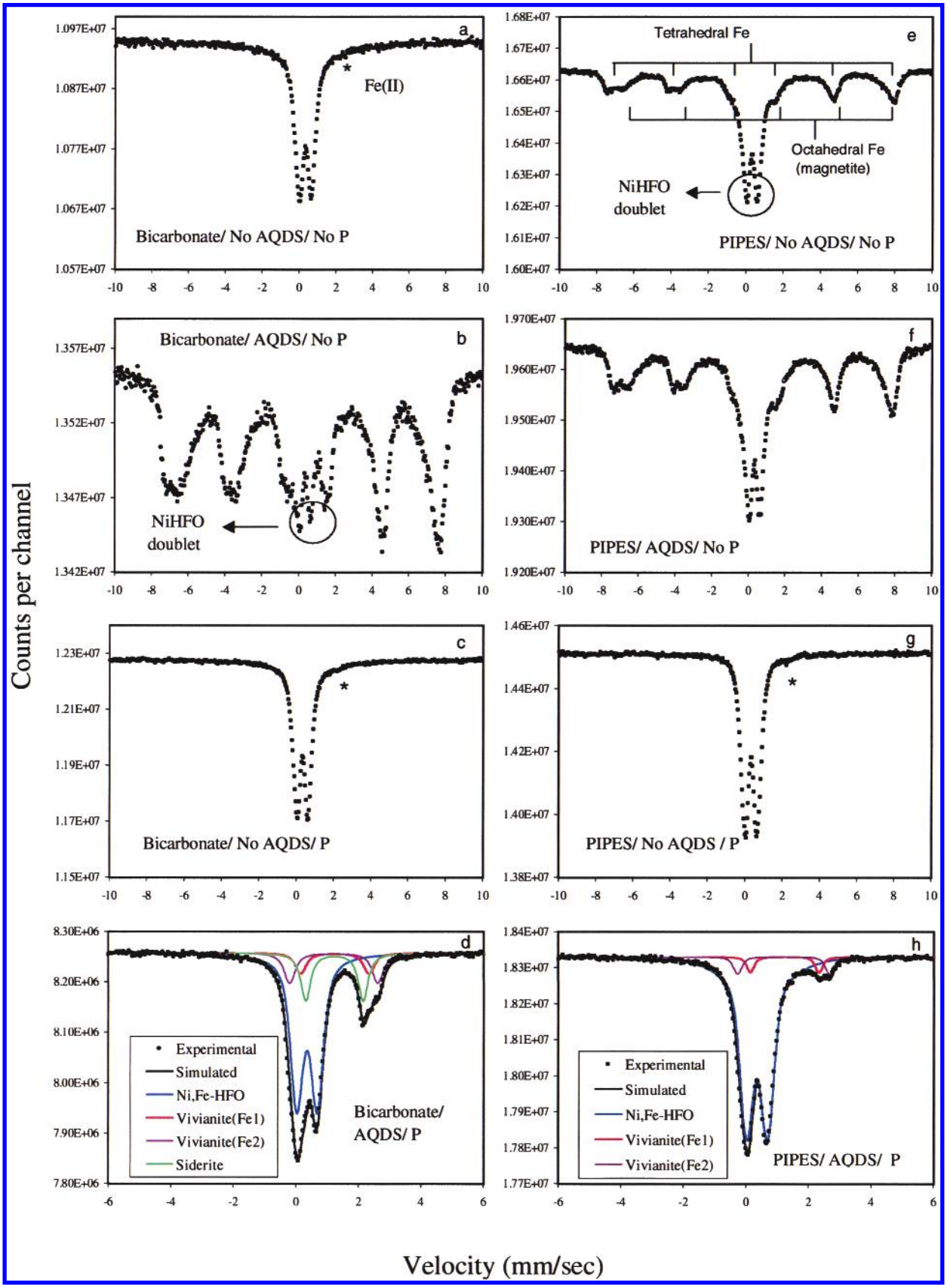

FIGURE 5. Mössbauer spectrum of bioreduced NiHFO (32 d) in PIPES or bicarbonate-buffered solutions.

Although divalent metal cations such as Zn^{2+} have been shown to function as inhibitors of ferric reductase activity in *Azotobacter vinelandii* (*26*), our experiments indicated that the impacts of Ni^{2+} on the bioreduction of HFO were not due to noncompetitive inhibition of the biological reduction process. Pretreatment of cells in solutions of 0.5 mmol/L $NiCl_2$ had little impact on the reduction of either Fe(III)−NTA or HFO (Figures 6 and 7). Although the presence of exogenous Ni^{2+} inhibited Fe(III)−NTA reduction, the effects were much more pronounced for HFO. In this latter

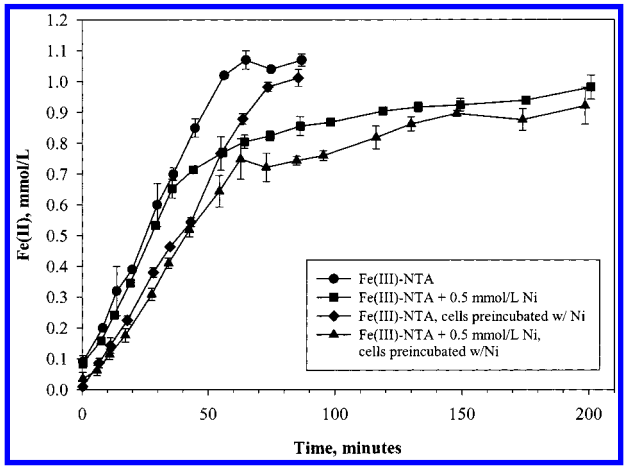

FIGURE 6. Influence of Ni^{2+} as 0.5 mmol/L $NiCl_2$ on the reduction of Fe(III)−NTA by *S. putrefaciens* CN32.

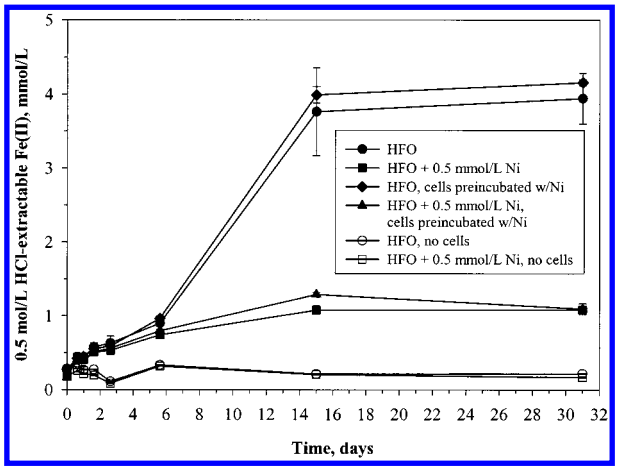

FIGURE 7. Influence of Ni^{2+} as 0.5 mmol/L $NiCl_2$ on the reduction of HFO by *S. putrefaciens* CN32.

experiment, the Ni^{2+} was strongly sorbed by HFO, indicating that sorbed Ni^{2+} may block sites on HFO used for electron transduction by DIRB. In contrast, Ni^{2+}, at 100 μmol/L, had no effect on the rate or extent of enzymatic reduction of U(VI) by *Desulfovibrio desulfuricans* (*27*). These results point to physical−chemical effects (e.g., surface site blockage, dissolution inhibition) as the dominant factors controlling the extent of NiHFO reduction and biomineralization.

Effects of AQDS and PO_4^{3-} on Bioreduction. Particularly striking were the interactive effects of AQDS and PO_4^{3-} on the bioreduction process; the presence of AQDS significantly enhanced the extent of NiHFO bioreduction regardless of whether PO_4^{3-} was present or not in either buffer (Figure 2) while the presence or absence of PO_4^{3-} markedly influenced biomineralization (Figures 4 and 5). AQDS has previously been shown to function as an electron shuttle between DIRB and iron(III) oxides, facilitating the rate and extent of reduction and relieving the requirement for cell−oxide contact (*4*, *7*, *28*, *29*). One exception to this was the lack of enhanced reduction of either Ni(II)- or Co(III)-substituted (at approximately 1%) goethite by *S. putrefaciens* (*2*). The reason for the lack of enhanced reduction were unclear but may have been due to the Ni^{2+} and Co(II/III) blocking goethite surface sites, slowing AH_2DS-facilitated reduction, similar to the ability of strongly sorbing metal cations to inhibit acid dissolution by reducing surface protonation (*30*, *31*).

AH_2DS because of its relatively high solubility, small size, and low $E°$ (−184 mV at pH 7) is a facile reductant of iron(III) oxides and may access surfaces and surface sites that bacteria cannot. The mechanisms by which DIRB reduce solid-phase Fe(III) are poorly understood. The localization of *c*-type cytochromes in the outer membrane of *S. oneidensis* (*32*, *33*) suggests that these organisms are able to establish a direct biochemical linkage between their electron transport system and the oxide surfaces. Therefore, the requirement for direct cell−oxide contact (*34*, *35*) likely limits electron transfer, and the presence of AQDS or humic acids can partially overcome this limitation until other factors become limiting. Although recent research suggests that some *Shewanella* sp. produce extracellular quinones that can function as electron shuttles (*36*), the extent to which microbial quinones facilitate iron-(III) oxide reduction is unknown.

Fe(II) sorption to oxide and cell surfaces has been implicated as an important factor controlling the rate and extent of bacterial reduction of iron oxides (*5*, *6*) and the presence of NTA to promote solubilization of Fe(II) enhanced the reduction of goethite in direct proportion to its concentration (*37*). The question therefore arises as to whether AQDS (or AH_2DS) can complex Fe(II) and, if so, whether this might have contributed to the enhanced bacterial reduction of iron oxides. Although the concentrations of soluble Fe(II) following bioreduction for 14 or 32 d were moderately higher in solutions with AQDS (but without PO_4^{3-}) than in its absence (Figure 3), it is clear that complexation effects could only account for a small fraction of the enhanced NiHFO reduction.

Although the presence of PO_4^{3-} did not markedly influence the extent of NiHFO reduction (Figure 2), it significantly impacted the concentrations of soluble Fe(II) and Ni^{2+}, lowering their respective concentrations relative to the same treatment without PO_4^{3-} in each case (Figure 3). The influence of PO_4^{3-} on Fe(II) and Ni^{2+} solubility is most likely due to adsorption effects (Figure 2) and its ability to complex these metals and precipitate as $Fe_3(PO_4)_2{\cdot}8H_2O$ (vivianite), $Ni_3(PO_4)_2{\cdot}8H_2O$, or possibly a mixture of these phases. The presence of vivianite in the bioreduced samples with AQDS and PO_4^{3-} was readily confirmed by Mössbauer spectroscopy (Figure 5, panels d and h). Ni^{2+} forms isostructural double phosphates, e.g., $Ni_3(PO_4)_2{\cdot}8H_2O$ (*38*), and can probably substitute for Fe(II) in vivianite. In previous studies with Co-(II), we precipitated vivianite in the presence of dilute (Fe:Co was 100) Co(II), removing 99.8 and 98.8% of the Fe(II) and Co(II), respectively. The resulting vivianite coprecipitate produced an XRD pattern that was indistinguishable from specimen vivianite (*2*). Ni^{2+} is likely to exhibit a behavior similar to Co(II) given the similarities in their ionic radii.

The most marked effect of PO_4^{3-} was on the biomineralization of NiHFO; in all cases where the bioreduction of NiHFO resulted in extensive conversion to a magnetite-like mineral (Figures 4 and 5, panels b, e, and f), the corresponding treatments with PO_4^{3-} lacked any evidence of magnetite (Figures 4 and 5, panels d, g, and h). Magnetite can form rapidly at pH values at and above neutrality over periods of hours by topotactic conversion of HFO following Fe(II)(aq) sorption (*39*, *40*). Magnetite was a common product of HFO bioreduction by CN32 in PIPES and bicarbonate buffers with AQDS also in the absence of PO_4^{3-} (*7*). Inorganic phosphate has been shown to severely inhibit the formation of magnetite from the oxidation of Fe(II) solutions, via a green rust intermediate, by either stabilizing the green rust precursor or inhibiting magnetite crystallization (*41*). A phosphate-to-iron ratio of 0.4 was sufficient to inhibit the nucleation and crystal growth of magnetite from Fe(II) solutions being oxidized by nitrate under basic conditions (*42*). In our NiHFO (or HFO) bioreduction experiments, phosphate, present at a P:Fe ratio of ~0.1, probably inhibited magnetite formation via similar mechanisms—sorption to HFO and subsequent blockage of Fe(II) binding or via inhibition of magnetite crystallization. As shown in Figure 1, 88% of the added PO_4^{3-} was sorbed by the NiHFO at pH 7. It is of interest that the

TABLE 1. Comparison of Extent of Reduction of HFO and NiHFO by *S. putrefaciens* CN32 and Nature of Biominerals Formed

components	nominal % Fe(III) reduction[a]		% 0.5 mol/L HCl (NiHFO)[c]		phases identified	
	HFO[b]	NiHFO	Fe	Ni	HFO	NiHFO
PIPES	8.0	13.2	76.8	80.6	magnetite	NiHFO, magnetite
PIPES, P	29.1	10.3	91.9	91.7	pc[d]	NiHFO
PIPES, AQDS	12.8	21.2	84.6	86.0	magnetite	NiHFO, magnetite
PIPES, P, AQDS	74.2	20.6	94.1	94.4	green rust	NiHFO, vivianite
$NaHCO_3$	34.7	11.2	83.5	82.4	magnetite, siderite	NiHFO, goethite
$NaHCO_3$, P	61.5	10.3	96.3	95.0	siderite, vivianite	NiHFO
$NaHCO_3$, AQDS	48.2	29.2	91.4	89.0	magnetite, siderite	magnetite, NiHFO
$NaHCO_3$, P, AQDS	74.8	25.3	92.7	91.4	siderite, vivianite	NiHFO, vivianite, siderite

[a] Determined on 0.5 mol/L HCl extractions of Fe(II). [b] From Fredrickson et al. (*7*). [c] Percent of total metal, as determined by 5.0 mol/L HCl extraction, extracted by 0.5 mol/L HCl extraction. [d] pc, poorly crystalline.

NiHFO in the PIPES and bicarbonate buffered solutions with PO_4^{3-} but without AQDS showed no evidence of vivianite by Mössbauer spectroscopy. Mössbauer is capable of detecting vivianite at mass concentrations as little as 1%, despite reduction of ~10% of the initial Fe(III) concentration (Table 1). The reasons for the lack of vivianite formation in these samples are unclear but are likely due to strong sorption of P to unreduced NiHFO. As the mass of NiHFO is reduced via bacterial reduction, PO_4^{3-} is released, the Fe(II) concentration increases, and the solubility of vivianite is exceeded.

Partitioning of Ni^{2+} during Bioreduction. The behavior of Ni^{2+} closely tracked that of Fe in all treatments (Figure 3). The bioreduction of NiHFO reduced the HCl extractability of Fe and Ni^{2+} to similar degrees (Table 1) with the decrease being a function of the extent of bioreduction and mineralization. In treatments where the NiHFO was extensively converted to magnetite (Table 1), the 0.5 mol/L HCl-extractable Fe and Ni^{2+} was significantly decreased. In treatments where biomineralization was minimal and products, if any, were acid-soluble Fe(II) phases such as siderite and vivianite, the 0.5 and 5.0 mol/L HCl extraction results were in close agreement. The one exception to this was the decrease in the 0.5 mol/L HCl extractability of Fe and Ni^{2+} in the bioreduced NiHFO sample from the bicarbonate buffer without P or AQDS between the 14- and 32-d samplings (Figure 2 in Supporting Information); by day 32, 16−17% of Fe and Ni was not extractable by 0.5 mol/L HCl. The decrease in 0.5 mol/L HCl extractability of Fe and Ni in this treatment resulted from the Fe(II) catalyzed formation of goethite and 6-line ferrihydrite (Figure 4a). Both goethite and 6-line ferrihydrite are more resistant to weak acid dissolution than 2-line ferrihydrite.

We have found magnetite generated from the bioreduction of HFO to be highly soluble in 0.5 mol/L HCl probably due to the relatively small particle size (tens of nanometers) (*7*), but the rate and extent of acid dissolution of crystalline iron-(III) oxides such as magnetite can vary significantly for different specimens of the same oxide (*1*). Degree of crystallinity, particle size/surface area, and metal substitution all can influence acid dissolution of iron oxides.

The similarity in behavior of Ni and Fe suggests that Ni^{2+} was incorporated into the inverse spinel structure of magnetite. Previous studies have demonstrated that Ni^{2+} substitutes for Fe(II), due to similarities in ionic radii and electronegativity, in the octahedral sites of magnetite (*24*, *42*). Diamandescu et al. (*43*) reported synthesis of Ni-substituted magnetite ($Fe^{III}_2Fe^{II}_{(1-x)}Ni^{II}_xO_4$, $x = 0.256$). The congruent dissolution of Ni^{2+} and Fe from the 0.5 mol/L HCl extracts of samples where extensive biomineralization has occurred and the presence of Ni as revealed by EDS are indicative of Ni^{2+} substitution into magnetite and its more or less random distribution within the crystals (*1*). Cooper et al. (*12*) suggested that Zn^{2+}, which has an ionic radius of 0.75 Å as compared to 0.70 Å for Ni^{2+} and 0.74 Å for Fe^{2+}, was incorporated into magnetite during the bioreduction of lepidocrocite (α-FeOOH) with surface-bound Zn by *S. putrefaciens*.

Implications for Biomineralization and Trace Metal Mobility. The biomineralization of iron(III) oxides as they undergo reduction by DIRB is a complex process influenced by multiple biological and chemical factors. Among the major factors controlling Fe biomineralization is the composition and concentration of cations and anions, particularly those that can form complexes with Fe(II)(aq) or Fe(s) species or that function as counterions for precipitates (e.g., CO_3^{2-}, PO_4^{3-}). For example, the presence of PO_4^{3-} and carbonate promoted the formation of vivanite and siderite, respectively, during the bioreduction of Co(III)- and Ni^{2+}-substituted goethites (*2*). In fact, the presence of these inorganic ligands facilitated the reduction of the substituted goethites, probably by creating conditions where reduction was thermodynamically favored. In contrast, the current studies revealed that the presence of PO_4^{3-} stabilized NiHFO against mineralization during bioreduction while AQDS (without PO_4^{3-}) facilitated the conversion to magnetite. The current studies also showed minimal tendency for sideritization in HCO_3^- buffer, in contrast to our previous findings with unsubstituted HFO (*7*). The presence of coprecipitated Ni^{2+} may have slowed reduction, yielding conditions kinetically suited to magnetite formation.

Equally complex are the reactions that influence the solubility of trace metals such as Ni during the bacterial reduction of HFO coprecipitates. The bioreduction of NiHFO, in general, resulted in higher concentrations of Ni^{2+}(aq) [and Fe(II)(aq)], particularly in treatments that lacked PO_4^{3-}, as compared to unreduced NiHFO. Thus, for non-PO_4^{3-}-containing media there was net Ni^{2+} solubilization. While we have previously discussed the impacts of pH and PO_4^{3-} on Ni^{2+} solubility, other factors including carbonate complexation and solid/solution phase changes were influential as well. With respect to the bicarbonate issue, higher concentrations of both Ni^{2+}(aq) and Fe(II)(aq) were noted in bicarbonate buffer as compared to PIPES (Figure 3). While multiple causes were involved, e.g., pH and reduction extent, carbonate complexation also played a role. For example, the computed solubilities of $Ni(OH)_2$(c) (using data from refs *23* and *44*) were 3.28×10^{-3} and 6.46×10^{-4} mol/L at pH 7.2 in 30 mmol/L HCO_3^- and 30 mmol/L PIPES buffers, respectively, attesting to the role of bicarbonate complexation in Ni^{2+} solubilization.

In some treatments, bioreduction changed the character of the solid phase. The Ni-sorbing/host phase was depleted, and biogenic phases were formed with distinctly different and generally lower surface areas, adsorption strengths for Ni^{2+}, and distribution ratios for coprecipitation. Our previous studies have shown that biogenic siderite and vivianite crystallites are orders of magnitude larger in size than HFO (*7*). These phases and magnetite are unlikely to adsorb Ni^{2+}

comparably to HFO as their surface areas and chemical affinities for Ni^{2+} are smaller than HFO. This last point is to a large degree speculative but is supported by related publications (see, for example refs *45*−*48*). In addition to solid phase change, bioreduction has also enriched the aqueous phase with soluble Fe(II) that competes with Ni^{2+} for both surface and structural binding sites. Excess Fe(II)-(aq) has been shown to suppress Co(II)(aq) sorption to goethite, for example (*2*). Thus, it is to be anticipated that trace metal solubilization may be a common outcome of bioreduction unless large concentrations of precipitation inducing anions (e.g., 4.7 mmol/L PO_4^{3-}) are present.

An interesting comparison that speaks to (i) the comparative effects Fe(II)(aq) competition and HFO depletion and (ii) the challenge of quantitative interpretation can be made with the treatments presented in Figure 5, panels a (bicarbonate/no AQDS/no PO_4^{3-}) and b (bicarbonate/AQDS/no PO_4^{3-}). These two experiments displayed comparable final pH (6.88−7.25) and the highest concentrations of Ni^{2+}(aq) and Fe(II)(aq) (Figure 3) observed in all treatments. They differed markedly, however, in the composition of their final solid-phase assemblage (Figure 5). The bicarbonate/no AQDS/no PO_4^{3-} treatment showed no evidence for biomineralization (Figure 5a) while the bicarbonate/AQDS/no PO_4^{3-} treatment displayed the largest extent of biotransformation to magnetite (Figure 5b). Despite these dramatic differences, the final Ni^{2+}(aq) concentrations were almost identical, and correspondingly, so was the Ni_{total}/Fe_{total} ratio of the solid-phase residues, despite their different mineralogic composition. Speciation and solubility calculations showed that these final concentrations were over an order of magnitude below those saturated with $Ni(OH)_2$(c). Thus, their concentrations were not simply controlled by solubility equilibria of $Ni(OH)_2$(c). We speculate that the high final Ni^{2+}(aq) concentrations in the Figure 5a experiment resulted from the competitive displacement of sorbed Ni^{2+} by Fe-(II)(aq), while those in the Figure 5b experiment resulted from this same process occurring in combination with topotactic conversion to magnetite with concomitant fixation of Ni in the spinel structure. The magnetite formation in the experiment of Figure 5b was facilitated by the presence of AQDS. We suspect that sorption of Ni^{2+} to the biogenic magnetite was minimal due to the high Fe(II)(aq) concentrations and the low divalent metal complexation strength of the magnetite surface (*49*).

In the studied described here in, Ni was shown to inhibit dissimilatory microbial reduction of amorphous iron oxide via abiotic mechanisms, but the presence of other compounds such as humic acids or phosphate significantly modified the extent of bioreduction, metal solubility, and the suite of biominerals formed. AQDS, previously used as a model of humic acid quinone components, facilitated the immobilization of Ni within the crystal structure of biogenic magnetite. Accurate predictions of the biogeochemical behavior of trace metals in surface waters or groundwaters require thorough knowledge of the aqueous and solid-phase geochemical properties of the system in addition to the microbial processes.

Acknowledgments

This research was supported by the Natural and Accelerated Bioremediation Research Program (NABIR), Office of Biological and Environmental Research, U.S. Department of Energy (DOE). Pacific Northwest National Laboratory is operated for the DOE by Battelle Memorial Institute under Contract DE-AC06-76RLO 1830. We thank Alice Dohnalkova for excellent assistance on the HRTEM analyses and David Boone (Portland State University) for providing *S. putrefaciens* CN32 to us from the Subsurface Microbial Culture Collection.

Supporting Information Available

Mössbauer spectrum and XRD of unreduced NiHFO, concentrations of total Fe and Ni in 0.5 and 5.0 mol/L HCl extracts of bioreduced NiHFO, and transmission electron microscopy images of bioreduced NiHFO (4 pages). This material is available free of charge via the Internet at http://pubs.acs.org.

Literature Cited

(1) Cornell, R. M.; Schwertmann, U. *The Iron Oxides*; VCH: New York, 1996.
(2) Zachara, J. M.; Fredrickson, J. K.; Smith, S.; Gassman, P. *Geochim. Cosmochim. Acta*, **2001**, *65*, 75−93.
(3) Bousserrhine, N.; Gasser, U. G.; Jeanroy, E.; Berthelin, J. *Geomicrobiol. J.* **1999**, *16*, 245−259.
(4) Zachara, J. M.; Fredrickson, J. K.; Li, S. W.; Kennedy, D. W.; Smith, S. C.; Gassman, P. L. *Am. Mineral.* **1998**, *83*, 1426−1443.
(5) Roden, E. E.; Zachara, J. M. *Environ. Sci. Technol.* **1996**, *30*, 1618−1628.
(6) Urrutia, M. M.; Roden, E. E.; Fredrickson, J. K.; Zachara, J. M. *Geomicrobiol. J.* **1998**, *15*, 269−291.
(7) Fredrickson, J. K.; Zachara, J. M.; Kennedy, D. W.; Dong, H.; Onstott, T. C.; Hinman, N. W.; Li, S. W. *Geochim. Cosmochim. Acta* **1998**, *62*, 3239−3257.
(8) Lovley, R. R.; Phillips, E. J. P. *Appl. Environ. Microbiol.* **1987**, *53*, 1536−1540.
(9) Ford, R. G.; Bertsch, P. M.; Farley, K. J. *Environ. Sci. Technol.* **1997**, *31*, 2028−2033.
(10) Tessier, A.; Fortin, D.; Belzile, N.; DeVitre, R. R.; Leppard, G. G. *Geochim. Cosmochim. Acta* **1996**, *60*, 387−404.
(11) Winland, R. L.; Traina, S. J.; Bigham, J. M. *J. Environ. Qual.* **1991**, *20*, 452−460.
(12) Cooper, D. C.; Picardal, F.; Rivera, J.; Talbot, C. *Environ. Sci. Technol.* **2000**, *34*, 100−106.
(13) Ainsworth, C. C.; Plon, J. L.; Gassman, P. L.; Van Der Sluys, W. G. *Soil Sci. Soc. Am. J.* **1994**, *58*, 1615−1623.
(14) Dzombak, D. A.; Morel, F. M. M. *Surface Complexation Modeling: Hydrous Ferric Oxide*; John Wiley & Sons: New York, 1990.
(15) Lovley, D. R.; Phillips, E. J. P. *Appl. Environ. Microbiol.* **1986**, *52*, 751−757.
(16) Stookey, L. L. *Anal. Chem.* **1970**, *42*, 779−781.
(17) Rancourt, D. G.; Ping, J. Y. *Nucl. Instrum. Methods Phys. Res.* **1991**, *B58*, 85−97.
(18) Sidhu, P. S.; Gilkes, R. J.; Cornell, R. M.; Posner, A. M.; Quirk, J. P. *Clays Clay Miner.* **1981**, *29*, 269−276.
(19) Dong, H.; Fredrickson, J. K.; Kennedy, D. W.; Zachara, J. M.; Kukkadapu, R. K.; Onstott, T. C. *Chem. Geol.* **2000**, *169*, 299−318.
(20) Bancroft, G. M. *Mössbauer Spectroscopy: An Introduction for Inorganic Chemists and Geochemists*; McGraw-Hill: London, 1973.
(21) Greenwood, N. N.; Gibb, T. C. *Mössbauer Spectroscopy*; Chapman and Hall: London, 1971.
(22) Manning, P. G.; Ash, L. A. *Can. Mineral.* **1978**, *16*, 577−580.
(23) Mattigod, S. V.; Rai, D.; Felmy, A. R.; Rao, L. *J. Solution Chem.* **1997**, *26*, 391−403.
(24) Cornell, R. M.; Giovanoli, R.; Schneider, W. *J. Chem. Technol. Biotechnol.* **1992**, *53*, 73−79.
(25) Cornell, R. M.; Giovanoli, R. *Clays Clay Miner.* **1989**, *37*, 65−70.
(26) Huyer, M.; Page, W. J. *Appl. Environ. Microbiol.* **1989**, *171*, 4031−4037.
(27) Lovley, D. R.; Phillips, E. J. P. *Environ. Sci. Technol.* **1992**, *26*, 2228−2234.
(28) Lovley, D. R.; Coates, J. D.; Blunt-Harris, E. L.; Phillips, E. J. P.; Woodward, J. C. *Nature* **1996**, *382*, 445−448.
(29) Lovley, D. R.; Fraga, J. L.; Blunt-Harris, E. L.; Hayes, L. A.; Phillips, E. J. P.; Coates, J. D. *Acta Hydrochim. Hydrobiol.* **1998**, *26*, 152−157.
(30) Hering, J. G.; Stumm, W. In *Mineral−Water Interface Geochemistry*; Hochella, M. F., White, A. F., Eds.; Mineralogical Society of America: Washington, DC, 1990; Vol. 23, pp 427−465.
(31) Biber, M.; Dos Santos Afonso, M.; Stumm, W. *Geochim. Cosmochim. Acta* **1994**, *58*, 1999−2010.
(32) Myers, C. R.; Myers, J. M. *J. Bacteriol.* **1992**, *174*, 3429−3438.
(33) Myers, C.; Myers, J. *Biochim. Biophys.* **1997**, *1326*, 307−318.
(34) Lovley, D. R.; Phillips, E. J. P. *Appl. Environ. Microbiol.* **1988**, *54*, 1472−1480.
(35) Arnold, R. G.; DeChristina, T. J.; Hoffman, M. R. *Biotechnol. Bioeng.* **1988**, *32*, 1081−1096.
(36) Newman, D. K.; Kolter, R. *Nature* **2000**, *405*, 94−97.

(37) Urrutia, M. M.; Roden, E. E.; Zachara, J. M. *Environ. Sci. Technol.* **1999**, *33*, 4022−4028.
(38) Jambor, J. L.; Dutrizac, J. E. In *Process Mineralogy*; Hagni, R. D., Ed.; The Minerals, Metals and Materials Society: Warrendale, PA, 1995; pp 239−249.
(39) Cornell, R. M. *Clays Clay Miner.* **1988**, *23*, 329−332.
(40) Tronc, E.; Belleville, P.; Jolivet, J. P.; Livage, J. *Langmuir* **1992**, *8*, 313−319.
(41) Couling, S. B.; Mann, S. *J. Chem. Soc. Chem. Commun.* **1985**, 1713−1715.
(42) Sidhu, P. S.; Gilkes, R. J.; Posner, A. M. *J. Inorg. Nucl. Chem.* **1978**, *40*, 429−435.
(43) Diamandescu, L.; Mihaila-Tarabasanu, D.; Teodorescu, V.; Popescu-Pogrion, N. *Mater. Lett.* **1998**, *37*, 340−348.
(44) Fouillac, C.; Criaud, A. *Geochem. J.* **1984**, *18*, 297−303.
(45) Tamura, H.; Matijevic, E.; Meites, L. *J. Colloid Interface Sci.* **1983**, *92*, 303−314.
(46) Zachara, J. M.; Cowan, C. E.; Resch, C. T. *Geochim. Cosmochim. Acta* **1991**, *55*, 1549−1562.
(47) Tamura, H.; Katayama, N.; Furuichi, R. *J. Colloid Interface Sci.* **1997**, *195*, 192−202.
(48) Tamura, H.; Furuichi, R. *J. Colloid Interface Sci.* **1997**, *195*, 241−249.
(49) Criscenti, L. J.; Sverjensky, D. A. *Am. J. Sci.* **1999**, *299*, 828−899.

Received for review July 18, 2000. Revised manuscript received November 13, 2000. Accepted November 16, 2000.

ES001500V